GSI Annual Report 2004 (extracts)

Chemistry ('Chemistry and Superheavy Element Research')

On the production and chemical separation of Hs (element 108) ***Page 2***
Dvorak, J.; Krücken, R.; Nebel, F.; Novackova, Z.; Türler, A.; Wierczinski, B.; Yakushev, A.; Brüchle, W.; Jäger, E.; Schimpf, E.; Schädel, M.; Semchenkov, A.; Kuznetsov, A.; Chelnokov, M.; Yeremin, A.; Düllmann, C. E.; Nagame, Y.; Eberhardt, K.; Thörle, P.; Dressler, R.; Qin, Z.; Wegrzecki, M.

Theoretical Investigations of the Reactivity of MO_4 and the Electronic Structure of $Na_2[MO_4(OH)_2]$, where M = Ru, Os, and Hs (element 108) ***Page 3***
Pershina, V.; Kratz, J. V.

Relativistic Effects on Volatility of Element 112 ***Page 4***
Pershina, V.; Bastug, T.; Fricke, B.; Sarpe-Tudoran, C.; Anton, J.

Calculations of the adsorption energies of element 112 and its homolog Hg on the Au(100) surface with improved basis sets ***Page 5***
Sarpe-Tudoran, C.; Pershina, V.; Fricke, B.; Anton, J.; Sepp, W.-D.

Relativistic Density Functional Calculations for (E114)X and PbX, where X = O, Pd, Pt, Au ***Page 6***
Sarpe-Tudoran, C.; Pershina, V.; Fricke, B.; Anton, J.; Sepp, W.-D.

The electrochemical deposition of Hg on various metal electrodes ***Page 7***
Hummrich, H.; Feist, F.; Kratz, J. V.

Separation of ^{211}Pb with ALOHA and subsequent electrochemical deposition ***Page 8***
Hummrich, H.; Feist, F.; Liebe, D.; Kratz, J. V.

Development of a separation scheme to search for ^{239}Cm Part I: The overall separation scheme
Qin, Z.; Brüchle, W.; Jäger, E.; Nayak, D.; Schimpf, E.; Schausten, B.; Schädel, M. ***Page 9***

Development of a separation scheme to search for ^{239}Cm Part II: The Cm separation modeled with lanthanide radiotracers ***Page 10***
Qin, Z.; Brüchle, W.; Jäger, E.; Nayak, D.; Schimpf, E.; Schausten, B.; Schädel, M.

Approaches to estimate the ionic radius of hydrated Po^{2+} ***Page 11***
Lyczko, K.; Bilewicz, A.; Brüchle, W.; Schausten, B.; Schädel, M.

Experimental Nuclear Structure, Astrophysics and Reactions

New results on synthesis of Hs isotopes ***Page 12***
Dvorak, J.; Krücken, R.; Nebel, F.; Novackova, Z.; Türler, A.; Wierczinski, B.; Yakushev, A.; Brüchle, W.; Jäger, E.; Schimpf, E.; Schädel, M.; Semchenkov, A.; Kuznetsov, A.; Chelnokov, M.; Yeremin, A.; Düllmann, C. E.; Nagame, Y.; Eberhardt, K.; Thörle, P.; Dressler, R.; Qin, Z.; Wegrzecki, M.

Search for the "missing" α-decay branch in ^{239}Cm ***Page 13***
Qin, Z.; Ackermann, D.; Brüchle, W.; Hessberger, F. P.; Jäger, E.; Kuusiniemi, P.; Münzenberg, G.; Nayak, D.; Schimpf, E.; Schädel, M.; Schausten, B.; Semchenkov, A.; Sulignano, B.; Eberhardt, K.; Kratz, J. V.; Liebe, D.; Thörle, P.; Novikov, Y. N.

Instruments and Methods (TASCA)

Envisaged TASCA configuration ***Page 14***
Semchenkov, A.; Brüchle, W.; Jäger, E.; Schimpf, E.; Schädel, M.; Türler, A.; Yakushev, A.; Gregorich, K. E.

3D magnetic measurements and field simulation of the TASCA C-magnet ***Page 15***
Belyakova, T.; Kukhtin, V.; Lamzin, E.; Sytchevsky, S.; Jäger, E.; Schimpf, E.; Schädel, M.; Semchenkov, A.; Moritz, G.; Mühle, C.; Klos, F.; Türler, A.; Yakushev, A.

On the production and chemical separation of Hs (element 108)

J. Dvorak[1], R. Krücken[1], F. Nebel[1], Z. Novackova[1], A. Türler[1], B. Wierczinski[1], A. Yakushev[1], W. Brüchle[2], E.Jäger[2] , E. Schimpf[2] , M. Schädel[2] , A. Semchenkov[1,2], A. Kuznetsov[3], M. Chelnokov[3], A. Yeremin[3], Ch. E. Düllmann[4], Y. Nagame[5], K. Eberhardt[6], P. Thörle[6], R. Dressler[7], Z. Qin[2,8],M. Wegrzecki[9]

[1]TUM Garching; [2]GSI Darmstadt; [3]JINR Dubna; [4]LBNL Berkeley and UC Berkeley; [5]JAERI Tokai; [6]Universität Mainz; [7]PSI Villigen; [8]IMP Lanzhou, [9]ITE Warsaw

Chemical separation of Hs in the form of HsO_4 provides an excellent tool to study the formation reactions and nuclear structure of nuclei close to the deformed nuclear shells at Z=108 and N=162 due to a high overall efficiency and a very high purification factor. The first chemical identification of Hs as HsO_4 was performed by Düllmann et al. [1] at GSI in 2001. Seven decay chains were detected in a thermogradient detector and were attributed to the decay of ^{269}Hs and ^{270}Hs. Deposition temperatures of -44 ± 6°C and -82 ± 7°C and adsorption enthalpies of -46 ± 2 kJ/mol and -39 ± 1 kJ/mol were reported for HsO_4 and OsO_4, respectively.

Here we report on preliminary results of a recent Hs chemistry experiment performed at the GSI Darmstadt in December 2004. A rotating ^{248}Cm target wheel consisting of three arc-shaped segments with a target thickness of 788, 743 and 244 µg/cm^2 on 15-µm Be backing foils was irradiated with $^{26}Mg^{5+}$ ions to produce Hs isotopes. The third segment contained 2 % in weight of ^{152}Gd (30% enrichment) for the simultaneous production of α-decaying Os isotopes. A total beam integral of 3.48×10^{18} ^{26}Mg particles was accumulated during 12 days: 1.46×10^{18} at E_{lab} = 145 MeV and 2.02×10^{18} at E_{lab} = 135 MeV in the middle of the target. The experimental setup (Fig. 1) was similar to the one described in [1]. Recoil products were thermalized in a He/O_2 (10% of O_2) gas mixture in a recoil chamber heated to 400°C. The chemical reaction was completed at 650-700°C in a quartz column directly connected to the exit of the recoil chamber. Volatile Hs and Os tetroxides were formed and transported with the gas flow at room temperature to a detector setup. Two different gas flow rates of 1.8 l/min and 1.5 l/min were applied. The transport time through a Teflon™ capillary, 8 m in length, with an inner diameter of 2 mm was less than 2 s. The new detection system COMPACT (Cryo On-line Multidetector for Physics And Chemistry of Transactinides) was used. A temperature gradient from +20°C to -142°C was established along the detector channel which consisted of 2×32 single PIPS detectors (1×1 cm^2 in size). The distance between top and bottom arrays was 0.6 mm. The active detector surface covered 70% of the inner surface of the detector assembly The overall efficiency of the experimental apparatus was about 50%. Decay chains detected in the 145-MeV run are presented in [2].

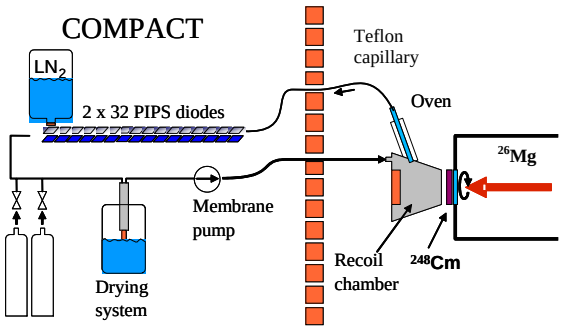

Fig. 1. Schematic of the experimental setup.

Figure 2 depicts the distribution of α-events with E_α = 4-5.1 MeV attributed to ^{172,173}Os along the detector as measured in the 145-MeV run. Seven events attributed to Hs isotopes are added to this plot (Fig. 2). The data are still being evaluated.

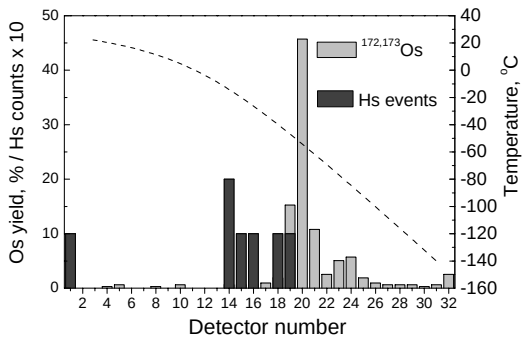

Fig. 2. Distribution of ^{172,173}Os and Hs isotopes in COMPACT.

References

[1] Ch.E. Düllmann et al., Nature **418**, 859 (2002).

[2] J. Dvorak et al., this Scientific Report, p.

Theoretical Investigations of the Reactivity of MO_4 and the Electronic Structure of $Na_2[MO_4(OH)_2]$, where M = Ru, Os, and Hs (element 108)

V. Pershina* and J. V. Kratz**
*GSI, Darmstadt
**Institut für Kernchemie, Universität Mainz

Recent experiments on the chemical identification of element 108, Hs, have delivered straightforward evidence that it belongs to group 8 of the Periodic Table [1]. In the presence of oxygen, Hs formed HsO_4 which was deposited in a gas-phase chromatography column at a temperature somewhat higher than that of OsO_4, thus confirming its chemical similarity with the latter and the high volatility. In more recent experiments [2] with volatile tetroxides, HsO_4 was shown to react with moisturized NaOH forming very probably the sodium hassate (VIII), $Na_2[HsO_4(OH)_2]$, by analogy with $Na_2[OsO_4(OH)_2]$ according to the reaction

$$2\ NaOH + HsO_4 \rightarrow Na_2[HsO_4(OH)_2]. \qquad (1)$$

In the present work, we study the reactivity of RuO_4, OsO_4, and HsO_4 with NaOH on the basis of results of the fully relativistic calculations for the components of the reaction of type (1) using the 4-component Density-Functional Theory method [3]. A model [4] was used to determine the free energy change ΔG^r of a reaction via changes in the ionic (ΔE^C) and covalent (ΔE^{OP}) contributions to the total binding energy. The latter are calculated using Mulliken effective charges Q_M and overlap populations, OP. It was shown that relative values of ΔG^r could be reliably predicted via the ΔE^C. The bond lengths (R_e) of the Os complex were taken from the experiment [5], and those of the Ru and Hs complexes were estimated using R_e for RuO_4 and HsO_4 with respect to $R_e(OsO_4)$ [6].

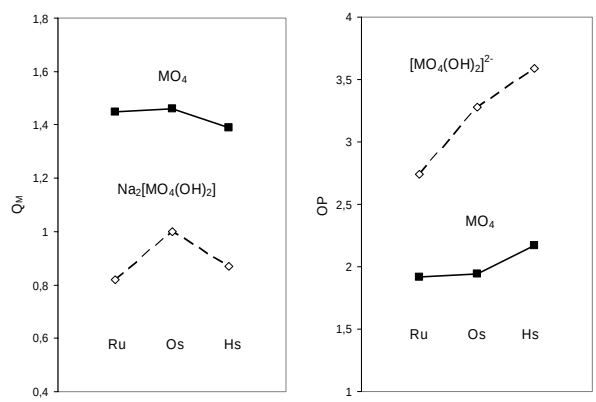

Fig. 1. Effective metal charges, Q_M, and overlap populations, OP, in MO_4 [6] and $[MO_4(OH)_2]^{2-}$ [this work] (M = Ru, Os, and Hs).

The values of Q_M and OP obtained for $[MO_4(OH)_2]^2$ and MO_4 are depicted in Fig. 1. They show $[HsO_4(OH)_2]^{2-}$ to be more covalent than the Os homolog, similarly to MO_4. Both Q_M and OP in $[RuO_4(OH)_2]^{2-}$ are significantly smaller than Q_M and OP of the Os and Hs anions, which is indicative for the fact that the Ru anion is not stable due to the weak ionic and covalent constituents of the bond strength. This is not the case with MO_4, where Q_M and OP of RuO_4 are very similar to those of OsO_4 (Fig. 1).

Table 1. Coulomb binding energies, E^C, for complexes of Ru, Os, and Hs and their differences, ΔE^C (in eV), for reactions of the complex formation

Complex/reaction	Ru	Os	Hs	Ref.
E^C: MO_4	-13.74	-13.86	-12.04	6
E^C: $[MO_4(OH)_2]^{2-}$	-3.58	-7.64	-5.26	this
E^C: $Na_2[MO_4(OH)_2]$	-5.70	-8.77	-6.41	this
ΔE^C: $MO_4 \Leftrightarrow [MO_4(OH)_2]^{2-}$	10.16	6.23	6.78	this
ΔE^C: $MO_4 \Leftrightarrow Na_2[MO_4(OH)_2]$	8.04	5.09	5.63	this

The obtained E^C for the species and ΔE^C for the complex formation reactions are given in Table 1. The values are similar for reactions of HsO_4 and OsO_4: HsO_4 should be slightly less reactive than OsO_4. We can give the upper limit of the difference in ΔG^r between HsO_4 and OsO_4 of 52 kJ/mol defined by the difference in their ΔE^C. (The slightly larger ΔOP=1.42 for the Hs reaction than ΔOP=1.34 for the Os reaction should slightly decrease this value). The values of ΔE^C for the reactions of RuO_4 are about 300 kJ/mol more positive than ΔE^C of the OsO_4 and HsO_4 reactions. The reason for that is the too low stability of the Ru complex anion manifested in its low E^C (low Q_M) and low E^{OP} (low OP) (Fig. 1). Thus, the so much more positive ΔG^r of the complex formation reaction of Ru compared to those of Os and Hs explains why $[RuO_4(OH)_2]^{2-}$ is not known. Finally, on the basis of these calculations, we predict the following trend for the formation of $[MO_4(OH)_2]^{2-}$, or $Na_2[MO_4(OH)_2]$ in group 8:

$$Os > Hs >> Ru.$$

The predicted slightly lower reactivity of HsO_4 as compared to that of OsO_4 has so far not clearly been revealed experimentally [2].

References

[1] C. Düllmann *et al.* Nature (Letters) **418**, 859 (2002).
[2] A. von Zweidorf, *et al*. A. Radiochim. Acta **92**, 855 (2004).
[3] S. Varga *et al*. Phys. Rev. A **59**, 4288 (1999).
[4] V. Pershina, Radiochim. Acta **92**, 455 (2004).
[5] N. N. Nevskii, *et al*. Dokl. Akad. Nauk. **266**, 628 (1982).
[6] V. Pershina, *et al.* J. Chem. Phys. **115**, 792 (2001).

Relativistic Effects on Volatility of Element 112

V. Pershina,[*] T. Bastug,[**] B. Fricke,[***] C. Sarpe-Tudoran,[***] J. Anton[***]
[*]GSI, Darmstadt
[**] School of Physics, University of Sydney, Australia
[***] Theoretische Physik, Universität Kassel

Investigation of influence of relativistic (rel.) effects on properties of the heaviest elements, especially on volatility of element 112, is one of the most fundamental and interesting tasks. Volatility is usually measured as the adsorption temperature, T_{ads}, in a chromatography column from which the adsorption enthalpy, ΔH_{ads}, is deduced. The only way to "detect" rel. effects is to compare measurements with rel. *vs.* nonrelativistic (nr.) predictions. The aim of the present study is to show the influence of rel. effects on volatility of element 112 in comparison with that of Hg as adsorption on inert and metal surfaces.

Adsorption on inert surfaces. For adsorption on inert surfaces (a quartz column, or a metal column covered with ice), a trend in volatility of the group-12 elements could be predicted using the following equation for the dispersion interaction energy [2]

$$E(x) = -\frac{3}{16}\left(\frac{\varepsilon-1}{\varepsilon+2}\right)\frac{\alpha_{at}}{\left(\frac{1}{IP_{slab}}+\frac{1}{IP_{at}}\right)x^3}, \quad (1)$$

where IP_{slab} is the ionization potential of the surface atom, ε is the dielectric constant of the surface (slab) substance and x is the interaction distance. Substituting calculated rel. and nr. values of α and IP of Hg and element 112 into eq. (1) gives results of Fig. 1.

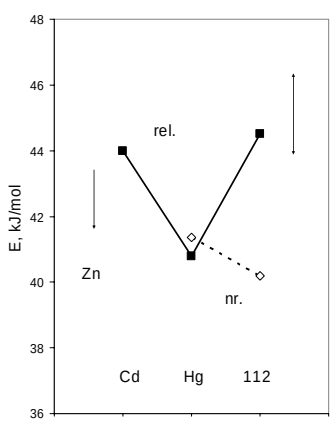

Fig. 1. Rel. and nr. dispersion interaction energies of the group-12 elements with quartz surface.

Thus, upon adsorption on an inert surface, element 112 will have the largest $E = -\Delta H_{ads}$ in group 12 and, hence, will be the least volatile. Non-relativistically, the trend is opposite.

Adsorption on metal surfaces. For the case of adsorption of element 112 and Hg on metal surfaces, e.g., Au(100), the influence of rel. effects on ΔH_{ads} could be different depending on the adsorption position – on-top, bridge or hollow – with respect to the surface atoms. In the on-top position, the main stereochemically active orbitals of Hg and element 112 are the ns and $np_{1/2}$, whose nr. and rel. R_{max} change in opposite ways in group 12. In the hollow position, the (n-1)d valence orbitals of these elements should be predominantly involved in bonding, whose rel. and nr. R_{max} change in the same way in the group. Present fully rel. and nr. 4c-DFT calculations for Hg and element 112 interacting with Au clusters of 14 and 9 atoms helped to elucidate this effect quantitatively. The results are summarized in Table 1 and Fig. 2.

Table 1. Rel. and nr. binding energies ($D_e = -\Delta H_{ads}$, eV) and optimized bond lengths (R_e, a.u.) for M-Au_{14} in the on-top and for M-Au_9 in the hollow positions (M = Hg and element 112)

Case	top		hollow	
	R_e	D_e	R_e	D_e
		Hg-Au_{14}		Hg-Au_9
rel.	5.0	0.86	3.8	0.85
nr.	5.5	0.64	4.6	0.41
		112-Au_{14}		112-Au_9
rel.	5.2	0.71	4.2	0.79
nr.	5.8	0.70	4.9	0.52

Thus, upon adsorption on the Au (100) surface, element 112 will be more volatile than Hg. Rel. effects do not increase $-\Delta H_{ads}$ of element 112 when adsorbed in the on-top position, while for the hollow position, rel. effects strongly increase the interaction energy, so that, relativistically, element 112 will be less volatile than nonrelativistically. The rel. and nr. ΔH_{ads} show opposite trends from Hg to element 112.

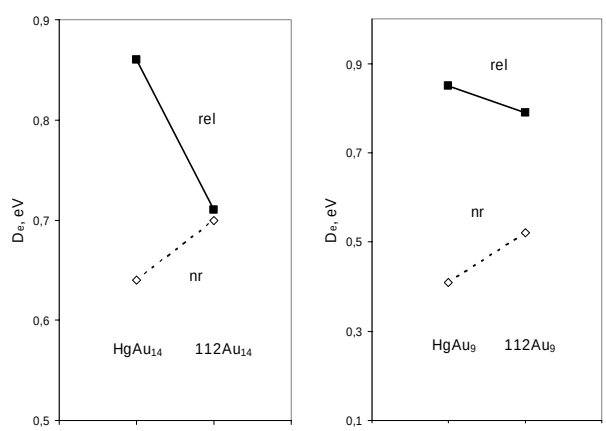

Fig. 2. Rel. and nr. binding energies (D_e, eV) for M-Au_{14} in the on-top position and for M-Au_9 in the hollow position (M = Hg and element 112).

Calculations of the adsorption energies of element 112 and its homolog Hg on the Au(100) surface with improved basis sets

C. Sarpe-Tudoran,* V. Pershina,** B. Fricke,* J. Anton*, W.-D. Sepp*
* Theoretische Physik, Universität Kassel
**GSI, Darmstadt

Within the framework of the theoretical study of the adsorption of element 112 and its homolog, Hg, on surfaces of transition-element metals [1-3], results of the improved calculations for ad-atom-gold cluster systems are reported here. The fully relativistic, 4-component Density Functional Theory (DFT) method [4] in its embedded cluster approximation was used for that purpose. For exchange-correlation effects, the Relativistic Local Density (RLDA) and General Gradient (BP88/P86), a higher level of theory, approximations were used. According to the embedding technique, the surface was simulated by a metal cluster embedded into an environment. This enables one to take effects of the environment explicitly into account and to achieve converged results with clusters of a moderate size.

In the calculations, inner clusters Au_m of m=14, 16, 22 and 29 atoms embedded in outer clusters of 112, 110, 92 and 156 atoms, respectively, were used to simulate the Au(100) surface. Hg and element 112 were considered in the on-top, bridge and hollow adsorption positions with respect to the surface atoms. The calculations were performed with two types of basis set: the set of type B includes the filled 1s through ns orbitals and virtual np and (n-1)f orbitals, while a more extended basis set of type B' includes the virtual nd, (n-2)g and nf orbitals in addition to those of the basis set B. Binding (adsorption) energies E_b of Hg and element 112 with clusters of various size and the different adsorption positions, calculated with the basis sets B and B', are shown in Fig. 1 and Table 1 (for the basis set B').

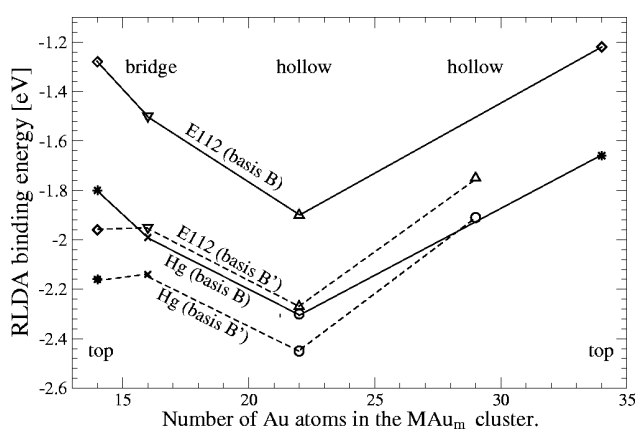

Fig. 1. The RLDA binding energies of element 112 and Hg with Au_m calculated for the basis set of types B and B'.

The results show that using the basis set B' improves E_b. Thus, E_b(B88/P86) for Hg in the preferential hollow position approaches the experimentally measured ΔH_{ads} = 101 kJ/mol (1.04 eV) [5].

Table 1. The RLDA and GGA(B88/P86) binding energies E_b and bond lengths r of Hg and element 112 with Au_m calculated for the basis set of type B'

m posit.	Approx.	$HgAu_m$		$112Au_m$	
		E_b, eV	r, a.u.	E_b, eV	r, a.u.
14 top	RLDA	2.16	4.82	1.96	5.10
	B88/P86	1.64	4.97	1.47	5.32
16 bridge	RLDA	2.14	4.30	1.95	4.50
	B88/P86	1.26	4.30	1.07	4.50
22 hollow	RLDA	2.45	3.50	2.27	3.80
29 hollow	RLDA	1.91	3.51	1.75	3.80
	B88/P86	0.86	4.11	0.72	4.37

The difference in the binding energies between Hg and element 112, E_b^{Hg}-E_b^{112}, stays almost the same for the basis set of type B or B', independently of m and the adsorption position (Fig. 2). Using the extended basis set B' instead of B brings this difference from ~0.4 eV down to 0.15 eV. A slight decrease in ΔE_b is also observed with increasing m.

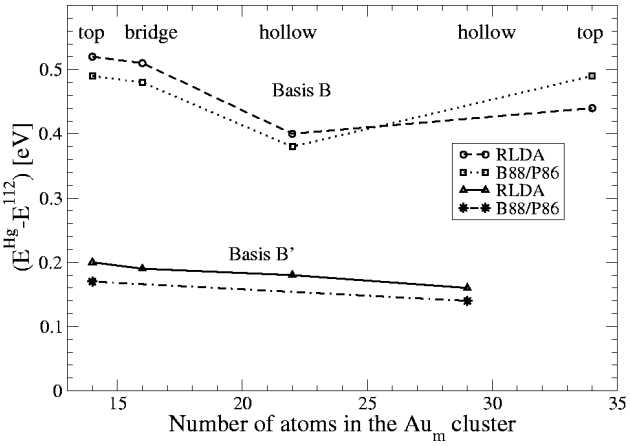

Fig. 2. The difference in the binding energies, E_b^{Hg}-E_b^{112}, between Hg and element 112 interacting with Au_m.

Thus, results of these calculations with the more extended basis set show that element 112 should be about 0.15 eV (15 kJ/mol) weaker adsorbed on the (100) Au surface than Hg, in agreement with our earlier conclusions made on the basis of the calculations for the Hg and 112 dimers [1,2].

References

[1] V. Pershina *et al*. *Chem. Phys. Lett.*, **365**, 176 (2002).
[2] V. Pershina, *et al*. *Nucl. Phys*. A **734**, 200 (2004).
[3] C. Sarpe-Tudoran, Doctoral Thesis, Kassel, 2004.
[4] T. Jacob, *et al*. *Surf. Sci.* **536**, 45 (2003).
[5] J.-P. Niklaus, *et al*. PSI Annual Report 2002, p. 8.

Relativistic Density Functional Calculations for (E114)X and PbX, where X = O, Pd, Pt, Au

C. Sarpe-Tudoran*, V. Pershina**, B. Fricke*, J. Anton*, and W.-D. Sepp*

* Universität Kassel, D-34109 Kassel; **Gesellschaft für Schwerionenforschung, D-64291 Darmstadt

The production of element $^{290}114$ with the half-life of 21 s [1] was reported by JINR, Dubna, Russia. Presently, chemical experiments are planned at GSI to prove the existence of E114 by its deposition on surfaces of transition-element metals. Element 114 is a closed-shell atom with an electronic configuration $7s^2 7p_{1/2}^2$. Due to the relativistic stabilization of the $7s$ and the $7p_{1/2}$ orbitals and the closed shell it is expected to be very inert. By now, only few calculations were done for element 114 and its compounds [2–6]. In the present work we consider some diatomic systems, with metal-metal ones serving as models for future cluster calculations.

In order to describe the molecular systems we use the 4-component non-collinear RDFT, in which the ground state energy is a unique functional of both electronic $[\rho]$ and magnetization density $[\vec{m}]$. The total energy of a molecular system is:

$$E = \sum_{i=1}^{M} n_i \langle \psi_i \mid \hat{t} \mid \psi_i \rangle + \int V^N \rho \, d^3\vec{r} + \frac{1}{2} \int V^H \rho \, d^3\vec{r} + E^{xc}[\rho, \vec{m}] + \sum_{p>q} \frac{Z_p Z_q}{|\vec{R}_p - \vec{R}_q|} .$$

Details of the method are given by Anton *et al.* [5].

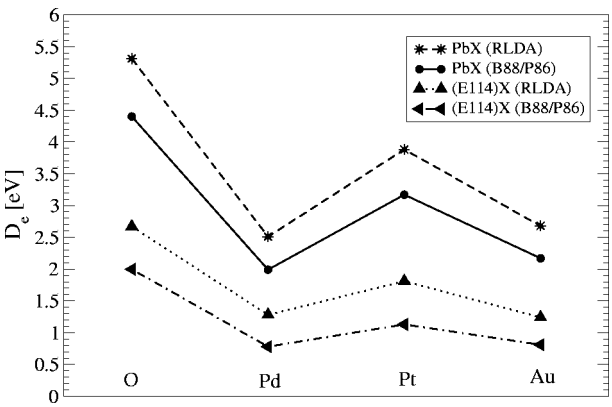

Figure 1: Dissociation energies for PbX and (E114)X, where X=O, Pd, Pt and Au.

Results of the calculations for PbX and (E114)X, where X = O, Pd, Pt and Au, as well as for Pb_2 and $(E114)_2$ are shown in Table 1. The obtained values for D_e, r and ω are in agreement with those obtained by Liu *et al.* for M_2 and MO [3]. By comparing with the experiment, one should keep in mind that spectroscopic constants are dependent on the experimental method. Thus, generally, agreement with experiment is quite satisfactory. The binding energies for the E114 compounds are all smaller than for the Pb compounds, showing that, indeed, element 114 is more inert than Pb. As the trend, $D_e^{MO} > D_e^{MPt} > D_e^{MAu} > D_e^{MPd}$ is predicted, where M = Pb and element 114. The bond lengths, r, increase from the Pb to E114 compounds.

Table 1: Binding energies (D_e), bond lengths (r) and vibrational frequencies (ω) for the PbX and (E114)X dimers, where X=O, Pd, Pt and Au.

		$D_e[eV]$	$r[a.u.]$	$\omega[cm^{-1}]$
Pb_2	RLDA	1.53	5.48	121.11
	B88/P86	1.16	5.62	108.58
	Exp. [6]	0.88	5.53	110.09
PbO	RLDA	5.31	3.62	747.08
	B88/P86	4.40	3.66	721.50
	Exp. [7]	3.87	3.63	721.00
PbPd	RLDA	2.50	4.62	222.61
	B88/P86	1.93	4.73	201.77
PbPt	RLDA	3.88	4.55	229.56
	B88/P86	3.17	4.63	213.49
PbAu	RLDA	2.68	4.88	167.17
	B88/P86	2.17	4.99	152.73
$(E114)_2$	RLDA	0.37	6.12	41.75
	B88/P86	0.13	6.60	25.85
(E114)O	RLDA	2.67	3.82	591.04
	B88/P86	2.00	3.89	536.34
(E114)Pd	RLDA	1.28	4.88	168.88
	B88/P86	0.78	5.07	137.82
(E114)Pt	RLDA	1.81	4.72	181.57
	B88/P86	1.13	4.83	157.37
(E114)Au	RLDA	1.24	5.17	116.44
	B88/P86	0.81	5.38	96.70

References

[1] Yu. Ts. Oganessian et al., *Phys. Rev. Lett.*, **83**, 3154, (1999); S. Hofmann, *et al.*, *Nucl. Phys. News*, **14**, 5-13, (2004).

[2] P. Schwerdtfeger, M. Seth, *J. Nucl. Radiochim. Sci.*, **3-1**, 133-136, (2002).

[3] W. Liu, C. van Wüllen, Y. K. Hahn, Y. J. Chi, and Y. S. Lee, *Adv. Quant. Chem.* **39**, 325 (2001).

[4] K. Balasubramanian, *J. Chem. Phys.*, **117**, 7426, (2002).

[5] J. Anton *et al.*, *Chem.Phys.*, in press.

[6] M. Heaven, T. Miller, V. E. Bondybey, *J. Phys. Chem.*, **87**, 2072-2075, (1983).

[7] K. P. Huber and G. Herzberg, *Molecular spectra and molecular structure* (Van Nostrand Reinhold, New York, 1979),Vol. 4.

The electrochemical deposition of Hg on various metal electrodes

H. Hummrich, F. Feist, J.V. Kratz

Institut für Kernchemie, Johannes Gutenberg-Universität Mainz, Germany

Recently, attempts were undertaken to chemically characterize element 112 in gas phase experiments [1].

A different approach involves experiments in the liquid phase. If we assume that element 112 is a noble metal (like its homolog Hg), a separation by electrochemical deposition on a metal electrode should be possible. Furthermore, this would result in an ideal sample for α-spectrometry.

In our experiments, we investigated the electrochemical deposition of Hg on various metal electrodes. A solution of $Hg(NO_3)_2$ in 0.1M HNO_3 was irradiated at the TRIGA reactor of the Mainz for 6h at a neutron flux of $7 \cdot 10^{11}$ n/s·cm² . The isotope ^{197g}Hg with a half live of 64,1h was produced with a specific activity of 70 kBq/mg, and its γ-line at 77 keV was evaluated in the experiments.

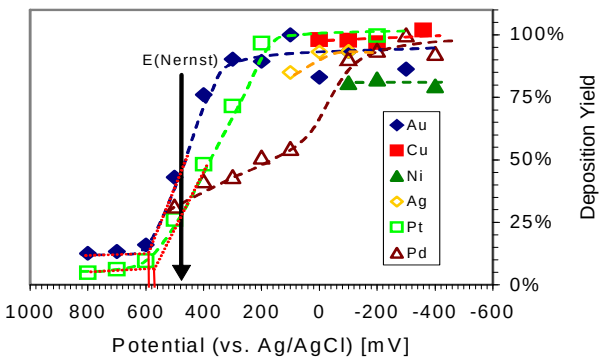

Fig.1: Electrodeposition yield vs. electrode potential for the deposition of ^{197g}Hg on various metal electrodes. In the experiments with Ag, Au, and Cu, 0.1M HNO_3 and with Pt, Pd, and Ni, 0.1M HCl was used as electrolyte

A heatable electrolysis cell with two working electrodes (total area 2 cm²), a Pt counter electrode and a Ag/AgCl reference electrode was used. The electrolyte volume of 1-2 ml was stirred with a high volume magnetic stirrer at 1000-1400 rpm. The total Hg concentration in each experiment was $5 \cdot 10^{-6}$ mol/l. This was low enough, so that the deposition still took place in the sub-monolayer region. 0.1 M HCl and 0.1 M HNO_3 were used as the electrolyte. The electrolysis time was 10 min. This should result in the maximum possible deposition for the given potential.

The electrodeposition yield was measured vs. the electrode potential (Fig. 1). The experiments, in which Ag, Cu, and Ni electrodes were used, were started at the potential that occured when the electrode is immersed into the solution (rest potential). At the rest potential, no current is applied. An increase of the potential beyond this rest potential would lead to a dissolution of the electrodes. For the deposition of Hg on Pt and Au, a critical potential at which a significant deposition starts, was deduced. For Pd, no well defined critical potential was found. For Cu, Ni, and Ag, the deposition is already nearly complete at the rest potential (spontaneous deposition).

In table 1, the critical potentials are compared with $E_{50\%}$-values, which were calculated with a microscopic-macroscopic model proposed by Eichler and Kratz [2] using thermodynamic properties of Hg and of the electrode material.

Table 1: Critical potentials for the deposition of Hg on various metal electrodes compared with theroetically predicted $E_{50\%}$ -values (all potentials vs. Ag/AgCl)

Electrode	E_{crit} [mV]	$E_{50\%}$ calc.
Au	+ 600	+ 710
Ni	> +50	+ 660
Ag	> +100	+ 620
Cu	> -100	+ 630
Pt	+ 580	+ 970
Pd	-	+ 1140

The electrodeposition speed was investigated for the deposition on Pd (20° and 80°) and Cu electrodes. Fig. 2 shows the decrease in activity vs. the electrolysis time. The $t_{50\%}$ - value is the time at which 50% of the activity is deposited. The electrodeposition seems to be faster on Cu electrodes than on Pd electrodes at room temperature. An increase in temperature lead to an increase in electrodeposition speed, in analogy to previous experiments with Pb [3].

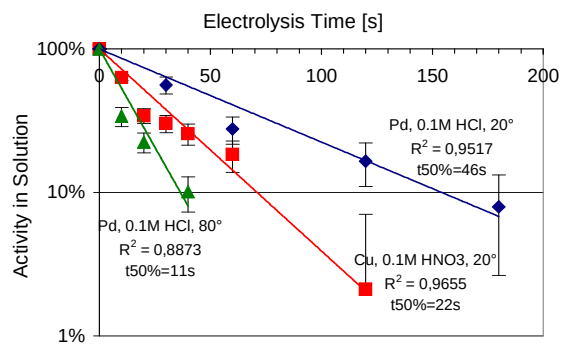

Fig.2: Electrodeposition speed vs. electrolysis time for the deposition of ^{197g}Hg on Pd and Cu. Electrolytic systems: Pd / 0.1M HCl / 20° / -500mV; Cu / 0.1M HNO_3 / 20° / -300mV; Pd / 0.1M HCl / 80° / -500mV

The obtained results will be taken into account in a beam time at GSI, where carrier-free Hg isotopes are produced via the reaction of ^{40}Ar with Sm. The transport of Hg with a KCl gas jet, the transfer into the liquid phase with the ALOHA system [4] and a subsequent electrodeposition will be investigated.

References

[1] S. Soverna et al, GSI, *Scientific Report 2003*, p. 187

[2] B. Eichler, J.V. Kratz, Radiochimica Acta **88,** 475 (2000)

[3] H. Hummrich et al., GSI, *Scientific Report 2003*, p. 199

[4] H. Hummrich et al, *this report*

Separation of ^{211}Pb with ALOHA and subsequent electrochemical deposition

H. Hummrich , F. Feist, D. Liebe, J.V. Kratz

Institut für Kernchemie, Johannes Gutenberg-Universität Mainz, Germany

To achieve a fast and (quasi)-continuous transfer of recoil atoms from the recoil chamber into the liquid phase, the ALOHA system was constructed and successfully used in chromatography experiments [1].

To prepare liquid phase experiments with element 114, the separation of its homolog Pb with ALOHA and its subsequent electrochemical deposition was investigated. A ^{219}Rn-emanating source was prepared by co-precipitation of ^{227}Ac with $Fe(OH)_3$. The source was placed in a 300 ml glass chamber where the 3,96s ^{219}Rn was allowed to decay. The daughter nuclides ^{211}Pb and ^{211}Bi were attached to KCl-clusters and transferred with a He flow of 2 l/min to ALOHA and deposited by impaction on a Ta disc. After impaction, the activity was stepped to the dissolution position and transferred to the electrolytic cell by continuously cyclic pumping of the electrolyte (0.1M HCl) with a low dead-volume HPLC pump. Fig. 1 shows the experimental set-up.

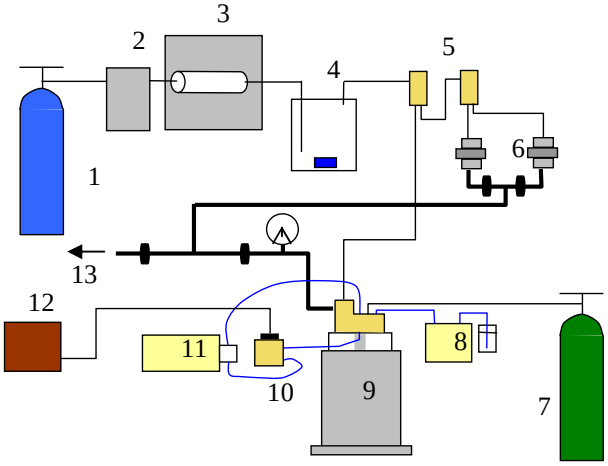

Fig.1: Experimental set-up. 1 Helium, 2 mass-flow-controller, 3 KCl cluster oven, 4 ^{227}Ac emanating source, 5 gas-jet switches, 6 direct catch and waste unit, 7 Nitrogen, 8 Acetone pump, 9 ALOHA, 10 electrodeposition cell, 11 electrolyte pump, 12 potentiostat, 13 to the ventilation sysem. Gas jet flow: black line, vacuum system: thick black line, liquid flow: blue line

The yield of impaction and dissolution in ALOHA (compared to a direct catch on a glassfiber filter) was measured via γ-spectrometry at different stepping times. Fig.2 shows that about 75 to 90% of the activity was successfully transferred from the gas-jet into the liquid phase using stepping times of 5s and longer. At lower stepping times, activity is lost due to the low dissolution volume.

For electrodeposition experiments with ^{211}Pb, a heatable electrolytic cell was attached to the ALOHA system. Pd was chosen as electrode material, 0.1M HCl as electrolyte. The deposition potential was –500 mV vs. Ag/AgCl.

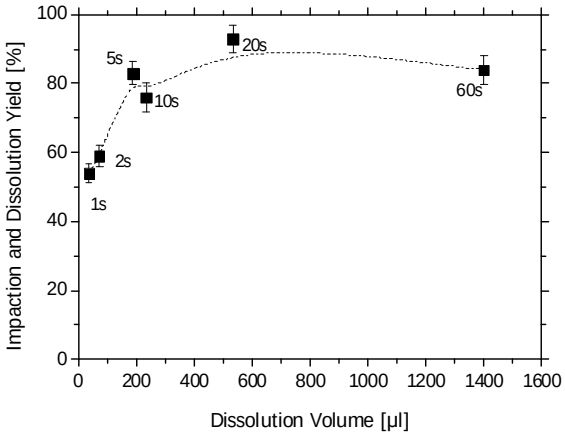

Fig.2: Impaction and dissolution yield for ^{211}Pb/^{211}Bi vs. dissolution volume (stepping time) with the ALOHA system, solvent 0.1M HCl

The activity was impacted for 10 min in the collection position, transferred to the dissolution position and dissolved. The deposition experiments were carried out at a temperature of ca. 75° and under vigorous stirring. At $t_{50\%}$=20s, 50% of the activity was deposited, as can be seen in Fig.3.

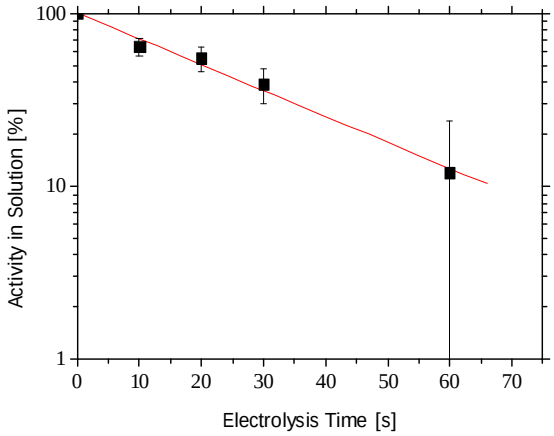

Fig 3: Electrodeposition of ^{211}Pb on Pd electrodes from 0.1M HCl at –500mV vs. electrolysis time.

The deposited activity could also be measured via α-spectrometry after the radioactive equilibrium between ^{211}Pb and ^{211}Bi was reached. Here, a 0.1 µm polycarbonate filter was used for the direct catch. In both cases, a FWHM of 60 keV for the 6,2 MeV line of ^{211}Bi was achieved

The presented system will be tested in a beam time at GSI with short lived Pb-isotopes in the reaction ^{40}Ar on Gd.

References

[1] A. Kronenberg et al., Annual Report, Institut für Kernchemie, Universität Mainz 2001, A4

Development of a separation scheme to search for ^{239}Cm
Part I: The overall separation scheme

Z. Qin[1,2], W. Brüchle[1], E. Jäger[1], D. Nayak[1,3], E. Schimpf[1], B. Schausten[1], M. Schädel[1]
[1]GSI, Darmstadt, Germany, [2]Institute of Modern Physics, Chinese Academy of Science, Lanzhou, P.R. China, [3]Saha Institute of Nuclear Physics, Kolkata, India

As radiochemical techniques have an unsurpassed sensitivity, they are best apt to search for, to identify and to determine very small α-decay branches of longer-lived transuranium nuclides. Therefore, we have developed a chemical separation scheme to search for the "missing" α-decay branch in ^{239}Cm ($T_{1/2} \approx 3$h). Details of the motivation for this experiment and preliminary results from the first experiments are given elsewhere in this report [1].

We decided to use Cu foils of 3.9 µm thickness, prepared by the GSI target laboratory, as a catcher material for ^{239}Cm. These Cu foils are thick enough to provide good mechanical stability and to catch all recoiling ^{239}Cm from the ^{232}Th (^{12}C, 5n) reaction. But they are thin enough to let large amounts of unwanted species, like the light fission products, pass through and to minimize the energy loss and heating from the passage of the ^{12}C beam. Cu also provides numerous advantages for the start of our chemistry to separate and prepare a clean Cm sample for a sensitive search for a very small α-branch.

Radiotracers of ^{153}Gd, ^{170}Tm, ^{153}Sm, ^{149,151}Pm and ^{147}Nd were obtained by irradiation of lanthanide (Ln) oxides or nitrates at the Mainz TRIGA reactor (thermal neutron flux ~ 10^{12} n cm^2/ s). They were used to develop the chemical separation scheme for actinides (An) consisting of a liquid-liquid extraction, a precipitation and a liquid chromatography (see Fig. 1), and to determine chemical yields.

The Cu catcher (≈ 20 mg Cu) was dissolved in 6 M HCl adding 2 drops of H_2O_2. To remove major activities produced in nuclear reactions with the Cu catcher, Ga and Ge were extracted quantitatively with 2,6-Dimethyl-4-heptanone. After adding 1 mg of La carrier Ln^{3+} and An^{3+} were precipitated with conc. NH_4OH while Cu remained in solution. The precipitate was dissolved in 500µl of 0.4 M HNO_3 which was fed into the sample loop of the liquid chromatography column. Details of the chromatographic separation of a Cm fraction, modeled with Nd, Pm, Sm and Gd tracer, can be found in Part II of this contribution.

The separated Cm fraction (Sm-Pm-fraction in Fig. 1) was rapidly evaporated on a Ta disk, which was heated from below by a hot plate. In addition, flowing hot He gas and an intensive IR-lamp were applied. This sample was suitable for α-particle pulse-height analysis to search for the α-decay of ^{239}Cm.

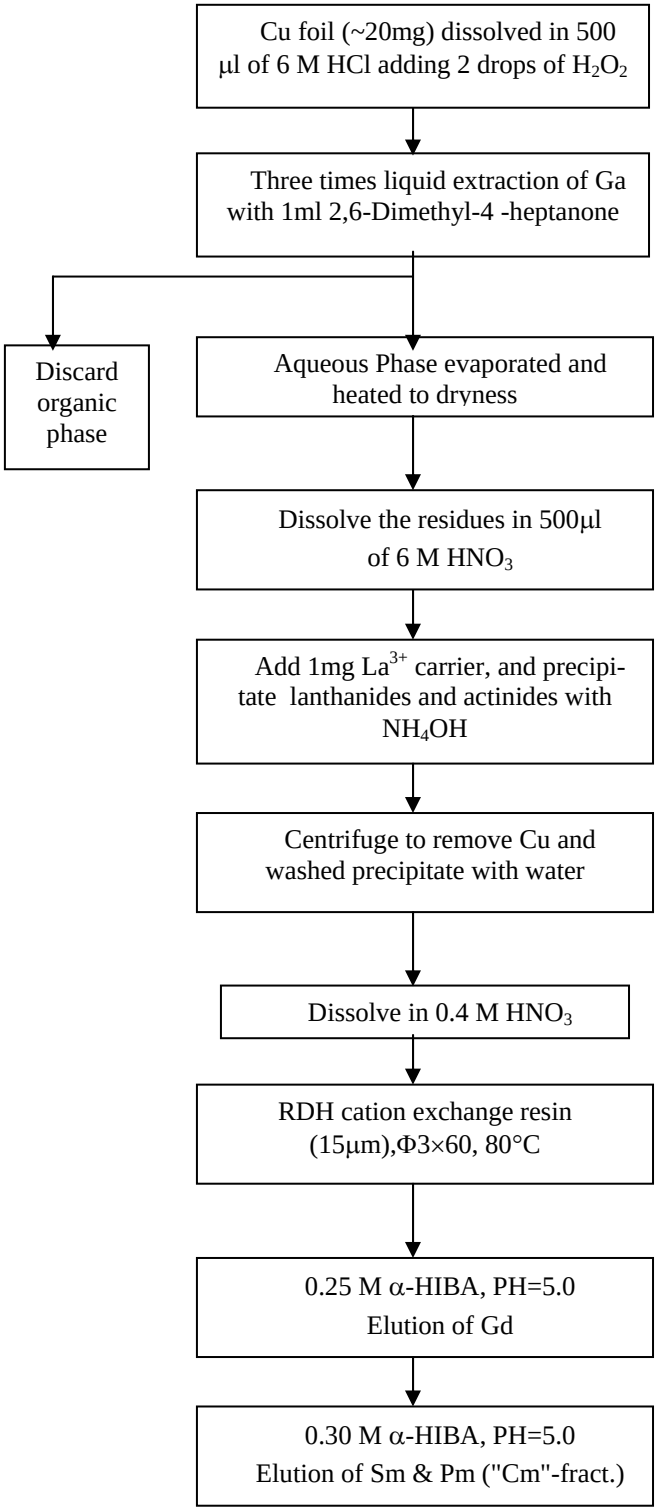

Fig. 1: The radiochemical separation procedure of a Cm fraction (Sm-Pm) from a Cu catcher foil.

Reference

[1] Z. Qin et al., GSI Scientific Report 2004.

Development of a separation scheme to search for ^{239}Cm
Part II: The Cm separation modeled with lanthanide radiotracers

Z. Qin[1,2], W. Brüchle[1], E. Jäger[1], D. Nayak[1,3], E. Schimpf[1], B. Schausten[1], M. Schädel[1]
[1]GSI, Darmstadt, Germany, [2]Institute of Modern Physics, Chinese Academy of Science, Lanzhou, P.R. China, [3]Saha Institute of Nuclear Physics, Kolkata, India

The overall separation scheme to obtain a chemically purified Cm sample for the search of an α-decay branch in ^{239}Cm (see [1] for preliminary results) is described in Part I of this contribution. This Part II describes details of the liquid chromatographic separation of a Cm fraction – modeled with lanthanide (Ln) tracers. The main goal of the scheme was to produce fast, reliably and with a high and controllable yield Cm fractions which are free from unwanted α-activities. This separation scheme was not optimized to separate elements which may strongly interfere in γ-spectroscopic studies.

One of the best known and most frequently applied separations of actinides (An) from each other is performed on cation exchange resin (CIX) utilizing differences in the complex formation of An^{3+} (Ln^{3+}) ions with (buffered) ammonium α-hydroxyisobutyrate (α-HIB) [2-4]. In comparative studies of the Ln and An separation [4] usually the elution position of Cm is taken as a reference and is normalized to 1. Elution positions for all other elements are, for a given system, given relative to Cm. For elutions with α-HIB from the CIX Dowex 50x12 at 87^{0}C literature [4] values for the trivalent actinides Bk, Cm and Am are 0.45, 1.0 and 1.4. As the trivalent lanthanides Gd, Eu, Sm, Pm, and Nd elute at position 0.28, 0.39, 0.71, 1.2, and 2.1 they are ideal tracers not only to develop but also to monitor a Cm separation.

Our separation was performed by High Performance Liquid Chromatography (HPLC). The HPLC set-up consisted of six chemical inert pumps that pumped various solutions through tubing (i.d. 0.3 mm) to the chromatography column. Pneumatic slider valves, controlled by a PC computer, were used to direct the flow of conditioning solutions to the column, to load the sample solution onto the column, and to apply the eluents for the separation. In test experiments, see Fig. 1, five drops per fraction were collected and were assayed for γ-ray activity with a shielded HPGe detector.

A water-jacketed chromatographic column (3 mm i.d., 60 mm long) was packed with a 15 µm particle size CIX (8% cross-linked from Riedel-de Haen, Seelze-Hannover) and was heated to 80^{0}C. The hydroxide precipitation of Ln and An (see Part I) was dissolved in 500 µL 0.4 M HNO_3, transferred into a sample loop and loaded onto the column. With a flow rate of 0.3 mL/min, used throughout the experiment, all lanthanides and actinides were strongly adsorbed on top of the column after 2 min. Thereafter, for conditioning, the column was washed (i) with water for 6 min (1.8 mL), (ii) with 0.5 M NH_4NO_3 (pH = 5) for 15 min (4.5 mL) to convert the resin into the NH_4^+ form, and (iii) with water again for 6 min (1.8 mL). Subsequently, the mobile phase was changed to 0.25 M α-HIB at pH=5 to clean the column from unwanted species before starting the Cm elution. A typical behavior of Tm and Gd in test separations is shown in Fig. 1. From the elution position of the ^{170}Tm tracer (K_d = 0.026) a column dead volume of 20 drops (0.46 mL) was determined.

After 8 min (100 drops) - the major part of ^{153}Gd was eluted at that time - the mobile phase was changed to 0.3 M α-HIB at pH=5. Fig. 1 shows elution curves of ^{153}Sm, ^{151}Pm and ^{147}Nd tracers from test experiments. Curium is expected to peak at about drop number 160. Cm fractions (80 drops) were collected starting from drop 120 (20 drops after changing to 0.3 M α-HIB). The overall chemical yield for Cm should be 70% or higher as determined from lanthanide tracers. It should be noted that no Cm-Am-separation was planned. The Cm fraction would contain relatively large amounts of Am if present. For sample preparation, the Cm fraction was evaporated to dryness (see Part I).

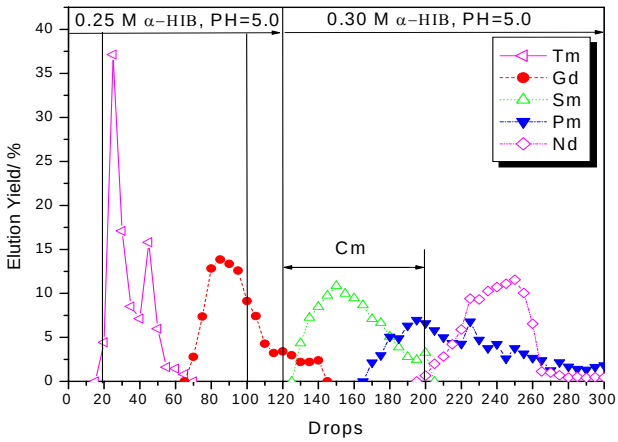

Figure 1. Elution curve of Gd, Tm, Sm, Pm, Nd with α-HIB.

After the Cm elution was finished, the column was stripped with 0.5 M α-HIB at pH=5 to remove the La^{3+} carrier, which was used for the precipitation described in Part I, from the resin. Subsequently, the column was regenerated by rinsing it with water and 0.4 M HNO_3 to prepare it for the next separation.

Reference

[1] Z. Qin et al., GSI Scientific Report 2004.

[2] G.R. Choppin et al., J. Inorg. Nucl. Chem. 2 (1956) 66.

[3] H.L. Smith and D.C. Hofmann J. Inorg. Nucl. Chem. 3 (1956) 243.

[4] G.H. Higgins, The Radiochemistry of the Transcurium Elements, U.S. National Academy of Science, Nuclear Science Series, NAS-NS-3031 (1960).

Approaches to estimate the ionic radius of hydrated Po^{2+}

K. Lyczko [1], A. Bilewicz[1], W. Brüchle [2], B. Schausten[2], and M. Schädel [2]

[1]Institute of Nuclear Chemistry and Technology, Warsaw, Poland; [2]GSI, Darmstadt, Germany

Due to the relativistic stabilisation of $6p_{1/2}$ electrons polonium – usually present in the 4+ oxidation state – can be reduced to the 2+ oxidation state. This cation has – outside it's filled $[Xe]4f^{14}5d^{10}$ electron shells - two electron pairs: $6s^2$ and $6p_{1/2}^2$. No information is available about the ionic radius of Po^{2+} and about it's coordination number of water molecules in aqueous solutions. The measurement of the ionic radius could be one first step towards a better understanding of the contribution of Po^{2+} electron orbitals to the chemical bonding.

The goal of our studies was to estimate the ionic radius of hydrated Po^{2+} from a comparison of the distribution coefficients (K_d) for Po^{2+} with K_d values of divalent metal cations of the second group of the Periodic Table (Ca^{2+}, Sr^{2+} and Ba^{2+}). This is based upon a well established linear correlation between reciprocal ionic radii (known for Ca^{2+}, Sr^{2+} and Ba^{2+}) and K_d values. This correlation is valid for ions with similar coordination numbers. K_d values can be obtained from the maxima of elution peaks in liquid-chromatography experiments. Earlier a cation exchange study of Po^{4+} in acid solutions ($HClO_4$, H_2SO_4, H_3PO_4, CH_3COOH and oxalic acid) has been reported [1].

We eluted polonium from the cation exchange resin Dowex 50W-X8, 200-400 mesh, with 3 M $HClO_4$ and 3.3 M CF_3SO_3H (triflic acid), both in SO_2 water solution. Perchloric acid and triflic acid were used because of their non-complexing properties for metal cations [2]. In order to reduce Po(IV) to Po(II) SO_2 was applied. It is commonly known that sulfur dioxide and hydrazine reduce polonium to oxidation state +2 in acidic solutions [3]. As we were using low-level radioactive tracer solutions of ^{210}Po the measurement of α-activity from these samples was mandatory. Therefore, we were only able to use SO_2 as a reducing agent. Using hydrazine was impossible due to white salt residues which appeared during the evaporation step for α-sample preparation.

The used radiotracers ^{47}Ca (40 Bq/mg) and ^{85}Sr (3.3 kBq/mg) were produced at the Mainz TRIGA reactor. While the Ca tracer had a very low specific activity, commercially available ^{133}Ba was carrier free. Tracer solutions were prepared by dissolving the irradiated oxides in perchloric acid and aliquots were loaded onto the column (46 mm length and 3.2 mm inner diameter). Elutions were performed at a rate of about 3.3 mL/min.

From the maxima of the elution position in 3M $HClO_4$ we determined K_d values of 2, 7 and 24 for $^{47}Ca^{2+}$, $^{85}Sr^{2+}$, and $^{133}Ba^{2+}$, respectively. The corresponding literature [4] values are 10.4, 13.4 and 25.1. Presumably, lower K_d values for Ca and Sr in comparison with values from [4] result from the use of relatively large amounts of carrier material in our experiment. It should also be noted here that our Ca and Sr elution curves were rather wide and exhibited considerable tailings. For the elution with 3.3 M CF_3SO_3H the K_d values were 11 for Sr and 37 for Ba.

Then we studied the behaviour of polonium during the elution using 3 M $HClO_4$ with and without SO_2. The elution curves for both solutions were similar. Peaks were very broad with maxima appearing only after 65-75 mL giving incomprehensibly large K_d values (~ 450-550). As an additional surprise, we measured a (too) large elution maximum of about 25 mL, corresponding to a K_d of ~ 150, with 3.3 M CF_3SO_3H in SO_2 water. One would not expect a large or any difference in the elution of Po^{2+} with 3.3 M CF_3SO_3H and 3 M $HClO_4$.

We interpret the large K_d values for polonium in both systems such that we were not able to reduce polonium effectively to the +2 oxidation state by SO_2. The observation of the different elution position in the two acids can possibly be explained by the oxidizing properties of $HClO_4$. In perchloric acid solution we most likely could not reduce Po(IV) to the lower oxidation states at all.

The next step in these experiments will be the application of hydrazine as a reductant when using γ-emitting ^{206}Po, or liquid scintillation counting to measure α-active ^{210}Po in solution.

References

[1] Ampelegova N. I., *Soviet Radiochem.* **17**, 52 (1974)

[2] Cotton F. A. et al., *Advanced Inorganic Chemistry*, 6-th Edition, J. Wiley & Sons (1999), Chapter 2

[3] Gmelin Handbook: *Po* Suppl. Vol. 1, part 11

[4] M.Marhol, *Ion Exchangers in Analytical Chemistry*, Czechoslovak Academy of Sciences, Prague (1981), p.493

New results on synthesis of Hs isotopes

J. Dvorak[1], R. Krücken[1], F. Nebel[1], Z. Novackova[1], A. Türler[1], B. Wierczinski[1], A. Yakushev[1], W. Brüchle[2], E.Jäger[2] , E. Schimpf[2] , M. Schädel[2] , A. Semchenkov[1,2], A. Kuznetsov[3], M. Chelnokov[3], A. Yeremin[3], Ch. E. Düllmann[4], Y. Nagame[5], K. Eberhardt[6], P. Thörle[6], R. Dressler[7], Z. Qin[2,8],M. Wegrzecki[9]

[1]TUM Garching; [2]GSI Darmstadt; [3]JINR Dubna; [4]LBNL Berkeley and UC Berkeley; [5]JAERI Tokai; [6]Universität Mainz; [7]PSI Villigen; [8]IMP Lanzhou, [9]ITE Warsaw

Synthesis and investigation of heavy nuclei close to the deformed nuclear shells at Z=108 and N=162, especially of the even-even nucleus ^{270}Hs, provide important data for comparison with theoretical predictions. Relatively long half-lives for alpha decay and spontaneous fission were predicted for these nuclei [1,2]. The first chemical identification and the study of nuclear decay properties of Hs isotopes was accomplished in 2001 [3,4]. Gas phase chemical separation of Hs isotopes in the form of volatile HsO_4 provides a highly selective and very efficient method of isolation. Here we report preliminary results of a recent Hs chemistry experiment performed at the GSI UNILAC accelerator to measure the excitation function of the reaction ^{26}Mg(^{248}Cm, xn)$^{274-xn}$Hs and to obtain additional information on the decay properties of Hs isotopes and their daughters. Based on calculated excitation functions, experiments at beam energies of E_{lab} = 135 MeV and E_{lab} = 145 MeV in the center of the target were carried out. The resulting excitation energies of 40 MeV and 49 MeV correspond to the predicted maxima of the 4n and 5n evaporation channel, respectively. The experimental procedure is decribed in [5]. Beam integrals of 1.46×10^{18} (145 MeV) and 2.02×10^{18} (135 MeV) ^{26}Mg ions were accumulated. A first, preliminary analysis of the data at 145 MeV revealed 7 decay chains attributed to the decay of Hs isotopes. These decay chains with observed α-particle or fission fragment energies in MeV, decay times, as well as detector number, top (T) or bottom (B) position and gas flow rates are presented in Figure 1. The probabilities that the observed decay chains are of random origin are low and comparable to the values given in [3,4]. The data accumulated at 135-MeV is currently being analyzed.

References

[1] I. Muntian et al., Acta Phys. Pol. B **32**, 691 (2001).
[2] R. Smolańczuk et al., Phys. Rev. C, **52**, 1871 (1995).
[3] Ch.E. Düllmann et al., Nature **418**, 859 (2002).
[4] A. Türler et al., Eur. Phys. J. A **17**, 505 (2003).
[5] J. Dvorak et al., this Annual Report, p.

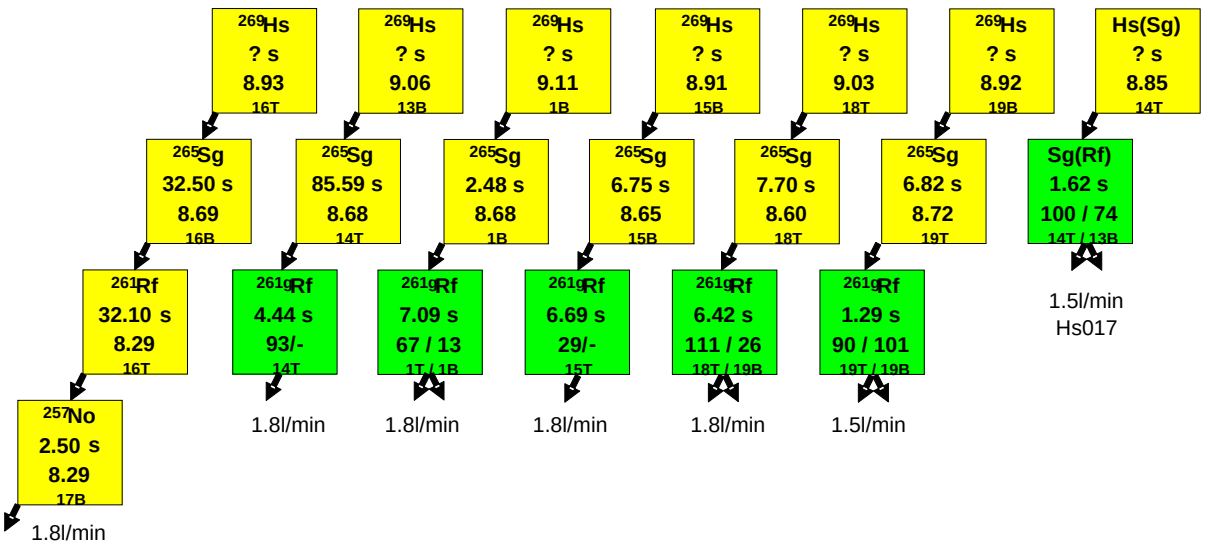

Figure 1. Correlated decay chains observed in the 145-MeV run.

Search for the "missing" α-decay branch in ^{239}Cm

Z. Qin [1,2], D. Ackermann[1,3], W. Brüchle[1], F.P. Hessberger[1], E. Jäger[1], P. Kuusiniemi[1], G. Münzenberg[1], D. Nayak[1,4], E. Schimpf[1], M. Schädel[1], B. Schausten[1], A. Semchenkov[1,6], B. Sulignano[1,3], K. Eberhardt[3], J.V. Kratz[3], D. Liebe[3], P.Thörle[3],Yu.N. Novikov[1, 5]

[1]GSI, Darmstadt, Germany, [2]Institute of Modern Physics, Chinese Academy of Science, Lanzhou, P.R. China,

[3]Johannes Gutenberg-Universität, Mainz, Germany, [4]Saha Institute of Nuclear Physics, Kolkata, India,

[5]Petersburg Nuclear Physics Institute, Gatchina, Russia, [6]Technical University of Munich, Germany

It is of special interest to search for those unknown α-emitters in the transuranium region which (i) are located along the path of α-decay chains that start in the super-heavy element region, and (ii) establish a link to nuclides with known masses. The knowledge of all Q_α values in an α-decay chain provides direct information on strongly desired mass values of SHE [1]. A search for the α-decay of ^{239}Cm was carried out at JAERI applying nuclear chemistry techniques [2]. Three α-events with an energy of 6.43±0.14 MeV were assigned to ^{239}Cm and the α/EC branching ratio was estimated as $(6.2 \pm 1.4)\times 10^{-5}$. However, due to this poor statistics, not only the α-energy was determined with an insufficient precision but also the isotope assignment remained questionable.

In our experiment, curium isotopes were produced in the reaction ^{232}Th(^{12}C,xn)$^{244-x}$Cm. Banana-shaped ^{232}Th targets were prepared by molecular plating at the University of Mainz. As a backing material, 5 μm thick Ti and 15 μm thick Be foils were used. Th target thicknesses were ≈ 700 μg/cm^2 on Ti and ≈ 900 μg/cm^2 on Be. $^{12}C^{2+}$ beams from the UNILAC were chosen such that after passing through a 20 μm Be vacuum window, He cooling gas of 200 mbar, and the backing material, the ^{12}C projectile energy was 74 MeV in the middle of the target. According to HIVAP calculations, this energy corresponds to the maximum of the excitation function for the reaction ^{232}Th(^{12}C,5n)^{239}Cm. Irradiations were performed with the rotating target wheel ARTESIA. Reaction products recoiling out of the target were implanted into 3.9 μm Cu catcher foils mounted 4 mm behind the rotating target wheel. Most fission fragments passed through the catcher because of their high TKE. To avoid overheating of the target and catcher material by the intensive ion beam, irradiations were carried out in a He atmosphere at 200 mbar. Each irradiation lasted ≈6 to 8 hours, and typical (particle) beam intensities varied between 0.3 μA during daytime and 0.85 μA at night. After irradiation, the copper catcher wheel was dismounted and was transported to a chemistry laboratory. The radiochemical separation procedure to prepare a purified Cm sample for α-spectroscopy was finished within 1.5 h or less. This procedure is described in a separate contribution to this report [3].

Two separate runs were carried out at the beginning and end of November. During the first run, targets with Th on Ti were used. They failed because of massive losses of target material from the Ti backing during the irradiation. Furthermore, ^{48,49,51}Cr, $^{43,44,46-48}$Sc, and ^{55,56}Co were produced from ^{12}C on Ti reactions with very high β- and γ-activities masking complementary γ-spectroscopic measurements. During the second run, targets with Th on Be foil were used which did not show significant Th losses. β and γ activities were about ten times lower than in the first run, and the nuclides mentioned above were not present.

In attempts to identify ^{239}Cm by γ-spectroscopic measurements, some samples were measured with a γ-x-detector and with a Ge-clover detector. γ-ray spectra dominantly showed lines from the decay of ^{153}Sm, ^{150,151}Pm and ^{147}Nd originating from fission of the compound nucleus. Cross sections for these isotopes are about 5 mb [4]. These activities from chemically not separated homologous rare earth elements did not allow identifying ^{239}Cm in the (single) γ-spectra or any Cm by characteristic x-rays. A further evaluation of coincidences is under way.

Samples were assayed for α-activities by 450 mm^2 PIPS detectors. The energy resolution of the evaporated samples was 60 keV. The α-events together with detector numbers and associated times were recorded and stored in list mode. Fig. 1 shows, for the first 10 h measuring time, the sum spectrum of five samples. As expected, ^{240}Cm (4n-channel, ≈100% α-decay) with α-energies of 6.29 and 6.24 MeV is dominant. Interestingly, there are some events around 6.5 MeV, close to the energy of ^{238}Cm (6n-channel). Data analysis and search for ^{239}Cm with a reported energy of 6.43 MeV [2] are in progress.

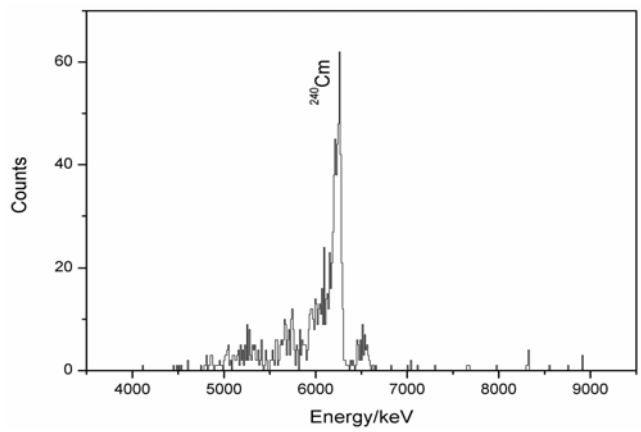

Fig.1 Sum α-spectrum of five samples (t_m =10 h each).

[1]G. Münzenberg. FRS Berichte, GSI (1995) (unpublished)

[2] N. Shinohara et al., JAERI-Review 2002-029, p. 45

[3] Z. Qin et al., GSI Scientific Report 2004

[4] A. Ramaswami et al., J. Radiochem. Nucl. Chem. 246 (2000) 225

Envisaged TASCA configuration

A. Semchenkov[1,2], W. Brüchle[1], E. Jäger[1], E. Schimpf[1], M. Schädel[1], A. Türler[2], A. Yakushev[2], K.E. Gregorich[3]
[1]GSI Darmstadt ;[2]TUM Garching; [3]LBNL Berkeley

The new **T**rans**A**ctinide **S**eparator and **C**hemistry **A**pparatus, **TASCA**, a new gas-filled recoil separator at the UNILAC, will use components of the former NASE [1]. As a typical reaction for design studies we took 5-6 MeV/u ^{48}Ca on a 0.5mg/cm^2 actinide target (^{238}U, ^{244}Pu). To find the best configuration, simulations were performed with the code TRANSPORT for a DQ_hQ_v (Fig1.), a DQ_vQ_h (Fig.2.), a Q_vDQ_h, and a $Q_vDQ_hQ_v$ (Fig.3.) structure (index **h** and **v** denotes focusing in horizontal and in vertical plane, respectively).

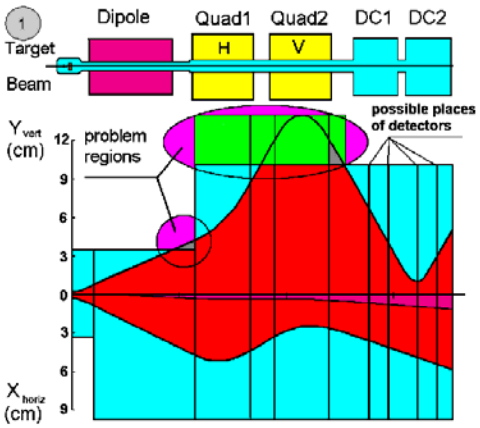

Fig.1. DQ_hQ_v simulations beam shape.

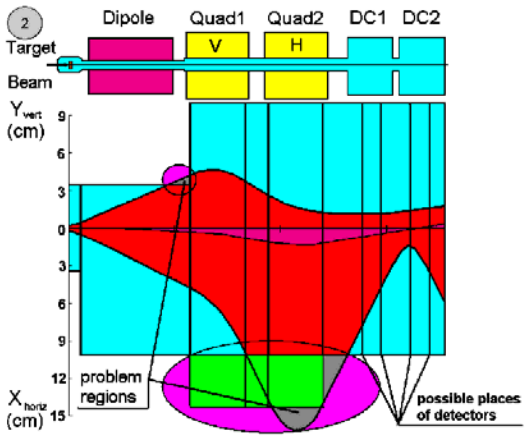

Fig.2. DQ_vQ_h simulations beam shape.

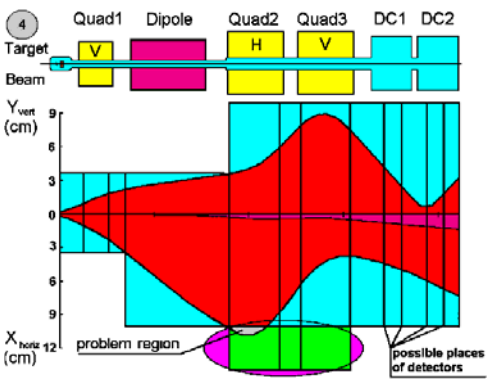

Fig.3. $Q_vDQ_hQ_v$ simulations beam shape.

We fixed the following ^{48}Ca beam parameters: Size x = y = ±2.5 mm, inclination x' = y' = 40 mrad and momentum dispersion ΔB=5%. Monte-Carlo simulations show [2] that 54% of all element 112 evaporation residues produced in the target are emitted within this angle and 92% within the assumed momentum bite. Therefore, a total transmission of about 50% seems reachable. The envelope of transmitted particles shows that, despite of losses at the end of the dipole magnet and in the Q_v vacuum chamber, we have the largest transmission in the DQ_hQ_v configuration and a 25 cm^2 image size; see Table 1. In the DQ_vQ_h arrangement products are lost in the dipole and the Q_1 vacuum chamber yielding a much lower transmission. However, a very small image size of 9 cm^2 is obtained. This can be advantageous when studying short lived isotopes. In a Q_vDQ_h configuration (not shown) a too large image size of 50 cm^2 is obtained. The $Q_vDQ_hQ_v$ set-up gives a horizontally and vertically well balanced shape, a large transmission, the largest dispersion and a 20 cm^2 image size. Figure 1 shows, that additional space from a new vacuum chamber, e.g. achievable with a rectangular tube inside the quadrupoles, would further increase the transmission of the DQ_hQ_v arrangement.

Instead of just using ± 40 mrad, final transmission calculation were made with those maximum beam inclinations which allow a full horizontal and vertical product acceptance with (i) the existing ("round") quadrupole vacuum chamber and (ii) "square" ones. Results are given in Table 1; for the square tubes normalized to a "round" solid angle. In essence, we opted for the DQ_hQ_v arrangement as a start for TASCA.

Table 1. Results of TRANSPORT simulations for different TASCA structures ("round" and "square" refer to different quadrupole vacuum chambers, x' and y' to the input inclination of the beam for simulations, and x'y' to the average inclination angle).

Structure	Dispersion	Acceptance	Trans.	Image size
DQ_hQ_v ("round")	0.7cm/ % L =3.5m	x'(y')=±80(±20)mrad, x'y'=±40mrad,	50%	S=25mm^2
DQ_hQ_v ("square")	0.7cm/% L =3.5m	x'(y')=±85(±30)mrad, x'y'=±50mrad,	55%	S=25mm^2
DQ_vQ_h ("round")	0.1cm/% L=3.5m	x'(y')=±20(±30)mrad, x'y'=±24mrad,	30%	S=9mm^2
DQ_vQ_h ("square")	0.1cm/% L=3.5m	x'(y')=±30(±30)mrad, x'y'=±30mrad,	36%	S=9mm^2
$Q_vDQ_hQ_v$ ("round")	1.1cm/% L=3.9 m	x(y)=±38(±40)mrad, x'y'=±39 mrad,	50%	S=20mm^2

References

[1] V. Ninov et al., Nucl. Instr. Meth. A 357 (1995) 486.
[2] K.E. Gregorich, private communication 2004.

3D magnetic measurements and field simulation of the TASCA C-magnet

T. Belyakova[1], V. Kukhtin[1], E. Lamzin[1], S. Sytchevsky[1], E. Jäger[2], E. Schimpf[2], M. Schädel[2], A. Semchenkov[2,3], G. Moritz[2], C. Mühle[2], F. Klos[2], A. Türler[3], A. Yakushev[3]
[1] Efremov Institute, St.Petersburg; [2]GSI Darmstadt; [3] TUM Garching

While preparing the new TASCA (**T**rans**A**ctinide **S**eparator and **C**hemistry **A**pparatus) project, 3D magnetic field measurements and simulations of the TASCA dipole magnet (C-type) were performed.

Measurements were carried out at GSI at coil currents of I=350, 600 and 700 A corresponding to magnetic field levels of B=1, 1.5 and 1.65 T, respectively. These 3D magnetic measurements, performed along the median and at planes ±25mm apart from it, will be used for trajectory simulations and magnet quality analysis.

The field calculations were made with the finite-element code KOMPOT [1,2]. KOMPOT simulates various 3D stationary field distributions. The code has rich graphic tools for building finite-element models and it can generate AutoCAD drawings. The postprocessor is capable of producing distributed and integral magnetic characteristics, for example, field maps or magnetic fluxes and EM forces for a given region. The graphical interface makes it possible to visualise calculated field distributions in any region of interest and compare it with measured GSI data.

The KOMPOT model developed for the TASCA C-magnet is presented in Fig. 1. The calculation model was reduced to one quarter of the magnet bordered by the median plane and the vertical symmetry plane. For both planes boundary conditions were given. The mesh had 128×63×59=475776 nodes. The mesh step in the working zone was taken as 6 mm along the horizontal axis and 4 mm along the vertical axis. 14 runs were carried out for the current varying from 50A to 700A with a 50A step. Fig. 2 and 3 illustrate field distributions at 700 A for typical cross sections.

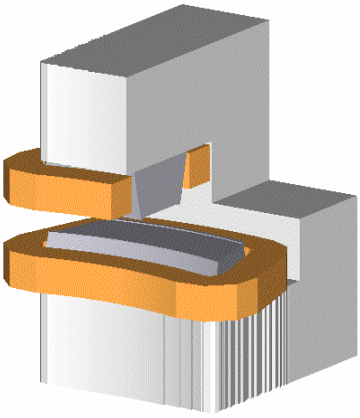

Fig.1. Computational model of the TASCA magnet

A comparison between measurements and simulations show a mismatch of less than 1%. Reasons are the unknown magnetic permeability curve for the existing magnet (a standard curve was used), some initial offset of the coordinate mesh of the measuring system from the magnet centre and non-symmetry of the real magnet assembly.

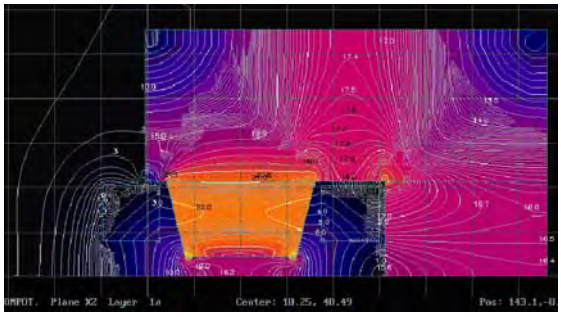

Fig.2. Induction [kG]. I=700amps. Vertical plane.

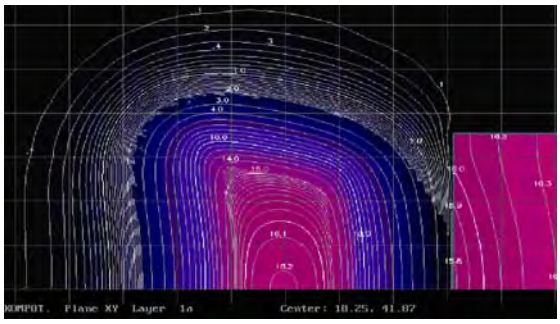

Fig.3. Induction [kG]. I=700amps. Median plane.

Computational model and magnetic measurement data allow us to calculate magnets with required magnetic field distributions. In addition, the synergism between model calculation and measurement will yield much better and much more economic results. Data of magnetic field simulations gives a possibility to have the 3D map of the field in the working area of the magnet for all required induction (current) region, which can be very useful for trajectory analysis.

As the next step we are calculating variants of pole pieces with anti-shims and new wider pole pieces in the frame of the existing coils in order to increase the maximum induction of the magnet and to provide a wide working area.

References

[1] A.Belov, et al., KOMPOT/M 1.0: computer code for 3D simulation of magnetostatic field in the analysis and synthesis of magnetic systems for electrophysical devices, RF Computer Program Register, Registration Certificate №2003612492, Moscow, Nov.12, 2003

[2] N.I.Doinikov, et al., On computation of 3-D magnetostatic fields of electrophysical apparatus magnet systems, IEEE Transact. On Magnetics, v.28, No.1, January 1992, pp.908–911